

## Supplementary Information

### Dirac-Cone induced Metallic Conductivity in $Cu_3(HHTP)_2$ : High-Quality MOF Thin Films Fabricated via ML-Driven Robotic Synthesis

Chatrawee Scheiger<sup>1</sup>, Jonas F. Pöhls<sup>2</sup>, Mersad Mostaghimi<sup>3</sup>, Lena Pilz<sup>1</sup>,  
Mariana Kozłowska<sup>3</sup>, Yidong Liu<sup>1</sup>, Lars Heinke<sup>4</sup>, Carlos Cesar Bof Bufon<sup>5</sup>,  
Thomas Weitz<sup>2,6</sup>, Wolfgang Wenzel<sup>3</sup>, and Christof Wöll<sup>1</sup>

<sup>1</sup>Institute of Functional Interfaces, Karlsruhe Institute of Technology,  
Hermann-von-Helmholtz-Platz 1, 76344 Eggenstein-Leopoldshafen,  
Germany

<sup>2</sup>Institute of Physics, Georg-August-University Göttingen,  
Friedrich-Hund-Platz 1, 37077 Göttingen

<sup>3</sup>Institute of Nanotechnology, Karlsruhe Institute of Technology,  
Hermann-von-Helmholtz-Platz 1, 76344 Eggenstein-Leopoldshafen,  
Germany

<sup>4</sup>Institute of Chemistry and Biochemistry, Freie Universität Berlin,  
Arnimallee 22, 14915 Berlin

<sup>5</sup>Institute of Geosciences and Exact Sciences, Department of Physics, São  
Paulo State University (UNESP), Rio Claro, SP, Brazil

<sup>6</sup>International Center for Advanced Studies of Energy Conversion  
(ICASEC), University of Göttingen, Germany

# Computational details

The fully relaxed structure of  $Cu_3(HHTP)_2$  MOF was obtained by the density functional theory (DFT) calculations, using Vienna Ab-initio Simulation Package (VASP) version 6.2.1[1]. The Perdew-Burke-Ernzerhof (PBE) functional and the projector augmented wave (PAW) method[2] were used for calculations. The cutoff energy of plane waves was set to 520 eV. The k-point mesh was set to 2x2x7. The structures were relaxed until the forces on the atoms were less than 0.01 eV/Å. The many-body dispersion energy with fractionally ionic model for polarizability method (MBD@rSC/FI) was used to include the dispersion correction [3, 4]. Collinear spin polarization calculations were considered.

Absorption spectra of structures extracted from periodic calculations were computed using the time-dependent density-functional theory (TD-DFT) method implemented in TURBOMOLE 7.7.1 software package[5, 6]. The resolution of identity (RI) approximation[7, 8, 9] has been applied. The spectra were calculated using the CAM-B3LYP functional[10] and the def2-TZVP basis set[9, 11, 12] based on 120 vertical excitations. The random phase approximation(RPA), and time-dependent DFT singlet excitation energies were used to calculate the absorption spectra[13]. All spectra were calculated in the gas phase. The computed absorption spectra were plotted using the Gaussian broadening function with a full width at half-maximum equal to 20 nm and a step width equal to 2 nm.[14] The electron density difference (EDD) upon the most intense excitations and the transition orbitals were analyzed as presented in Table 1 - Table 3.

Firstly, islands containing zero to three SBUs were extracted from a  $Cu_3(HHTP)_2$  single plane and the UV-vis spectra considering the saturated fragments (see Figures 11 - 13) were calculated. Secondly, two parallel layers of  $Cu_3(HHTP)_2$  were considered (Figures 14 - 19, either non-shifted, (labeled: parallel) or staggered (as in the 3D crystal structure) (labeled: sliding). With that, we were aimed to find out how the structure of the MOF and the formation of the stacked layers of  $Cu_3(HHTP)_2$  is connected to the spectral shift, especially for the band at around 575-625 nm.

# Analysis of UV-vis absorption of $Cu_3(HHTP)_2$

For single-plane (monolayer) and stacked plane models comprising linker monomers without bonded SBUs, we observed absorption bands below 300 nm (see Figure 1) originating from the HHTP linker. No peaks in the visible region occur. This characteristic optical transition corresponds to the catecholate  $\pi - \pi^*$  transition.

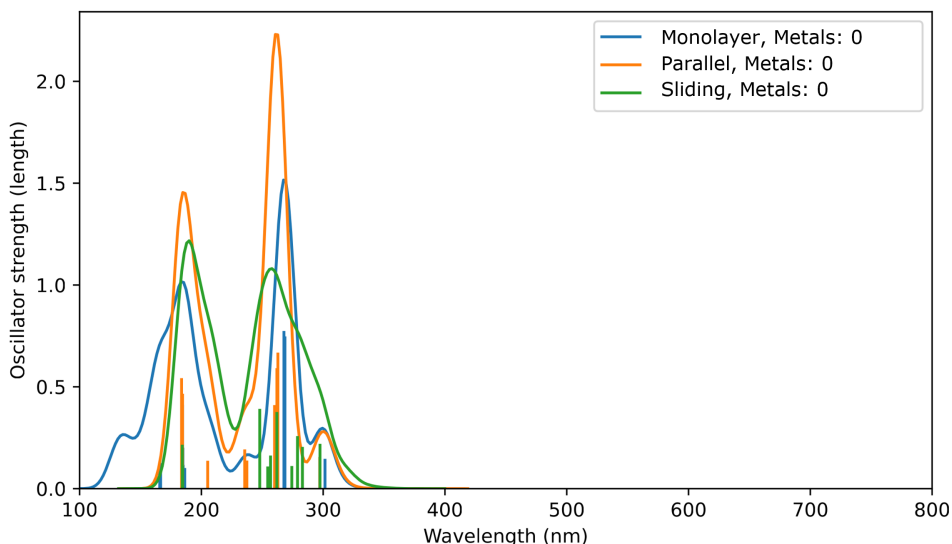


**Figure 1** – Absorption spectra of HHTP linkers extracted from periodic  $Cu_3(HHTP)_2$  as a monolayer and a double layer (i.e. stacked).

The spectra for systems comprising one linker and one SBU (Figures 11, 14 and 17) are depicted in Figure 2. We find that adding a metal significantly impacts the spectra. Specifically, a new absorption band between 500-600 nm appears. It is associated with the metal-linker charge transfer transition. In the inset figures, the electron density difference upon the marked excitation is depicted. The regions in blue and red correspond to electron donating and accepting regions, respectively. This change agrees with experiments since this band is present in UV-vis spectra of  $Cu_3(HHTP)_2$  in experiments. Note that the analysis of transition orbitals for the most intense absorption peaks is presented in the section below.

The absorption spectra in Figure 2 exhibit new peaks in the range around 300 nm since more components are included in the calculation and all contributions are explicitly accounted for. Small red-shift of the band between 300-400 nm is related to the change of electron density localization on HHTP due to binding to the SBU. Other spectral shifts are related to the layer formation and a slight change in the energy of transition molecular

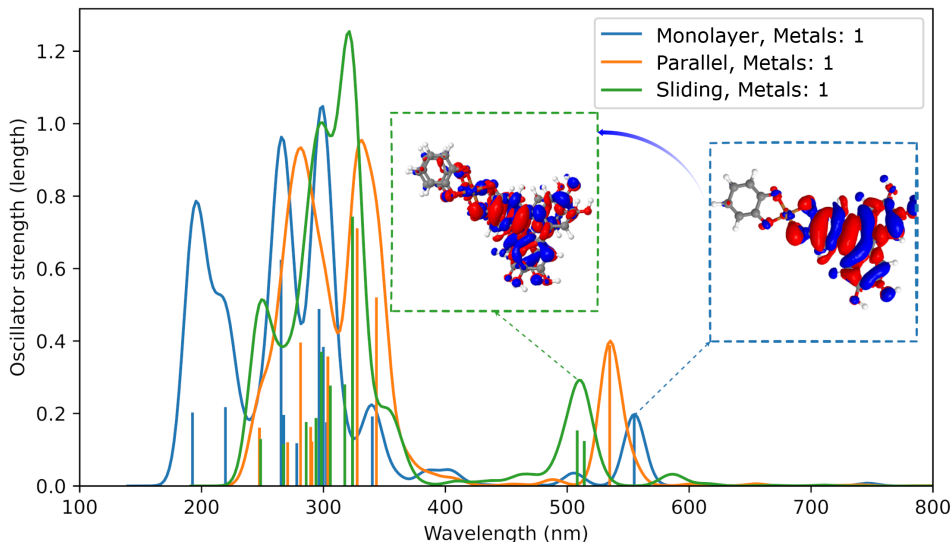


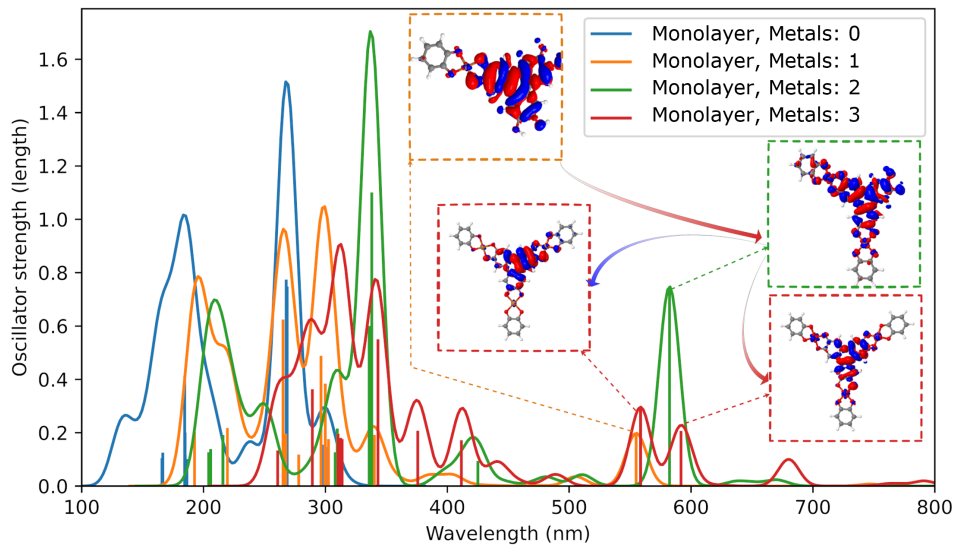
**Figure 2** – Absorption spectra for a monolayer, parallel, and sliding orientation structure of the HHTP island with one SBU. The peak around 580 nm is related to the metal-linker charge transfer contribution. The formation of the next layers shifts this band, but still this characteristic transition occurs between 500-600 nm.

orbitals and their contributions in electronic transitions.

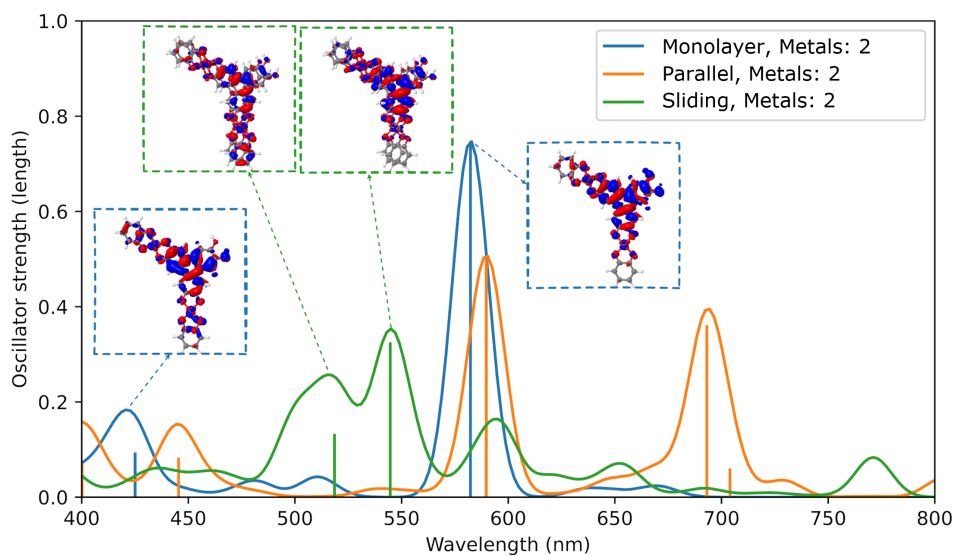
The next set of models included two and three SBUs in the extracted monolayer fragments (see Figure 3). Spectra were calculated to see how the consideration of more SBU-linker connectivities (i.e., changes in electron density delocalization due to more connections to SBUs) influences absorption spectra. It can be seen that there are minimal changes in the peak between 550-600 nm, but more changes occur in the UV region originated from the HHTP linker and the new peak in the low energy range appears when three SBUs are present. Moreover, much more absorption bands are visible with the increase in the number of SBUs in the system. Comparing this data with the experiment, we can conclude that the reduction of defects, in the sense of lacking non-SBU-coordinated linker sites should trigger more absorption in the visible range, appearing the sample to attain a darker (or black) color.

Considering the two SBUs in the stacked structures (see Figure 4), we see that the ABAB stacking (marked as sliding) introduces splitting of the band at approximately 580 nm and its red-shift and blue-shift simultaneously. This indicates highly sensitive nature of electronic transitions in the system and detectable changes in the structure using UV-vis absorption. Due to the complexity of the stacked systems with three SBUs, even more transitions happen (see Figure 5). Moreover, the multitude of transitions indicate high absorption of the calculated fragments within a wide spectral range. Excitations calculated with detailed explanation of transition orbitals to the most intense ones are listed below.

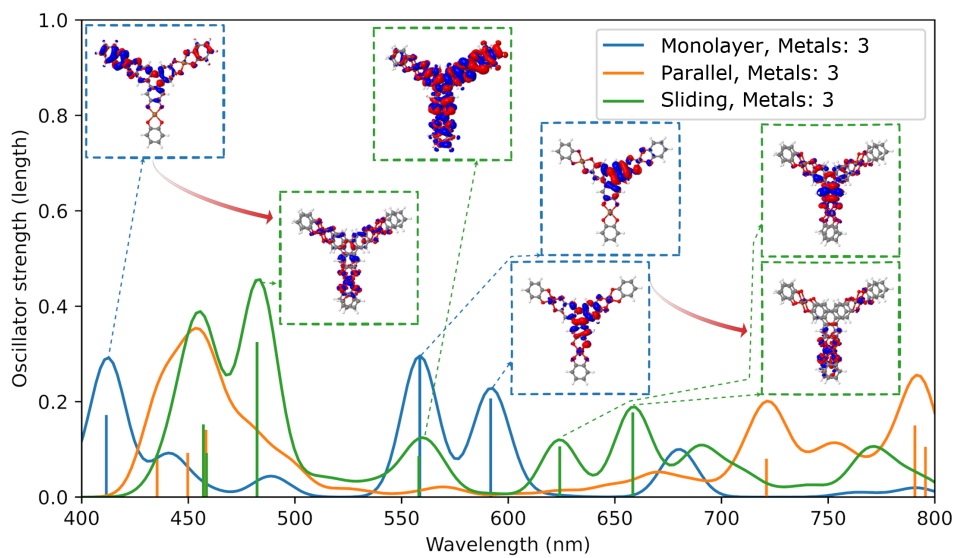
From the calculations performed, we observe that the binding of SBUs by HHTP linkers and stacking between MOF layers have a fingerprint in UV-vis spectra. It is connected to the electronic structure of the linker and its change upon binding to Cu-based SBUs. Less defective layers of  $Cu_3(HHTP)_2$  should possess several sets of absorption bands region with wavelengths longer than 400 nm.



**Figure 3** – Absorption spectra for a monolayer with zero, one, two, and three SBUs in the structure. This may show evidence of the color change of the samples to darker ones, i.e., with increased coordination, more absorption bands appear, therefore, less light is reflected.

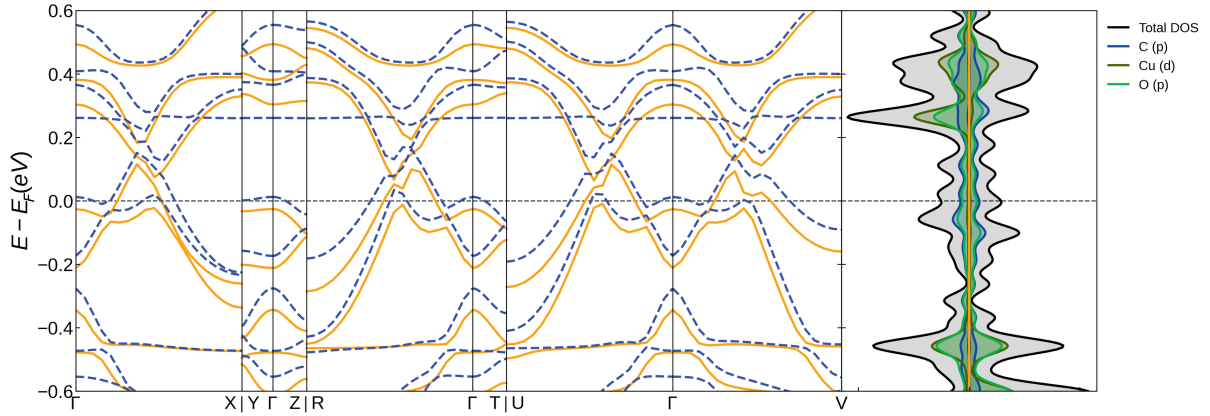


**Figure 4** – Absorption spectra for two SBU connected to the linkers models. The structures are in monolayer, parallel, and sliding orientation.

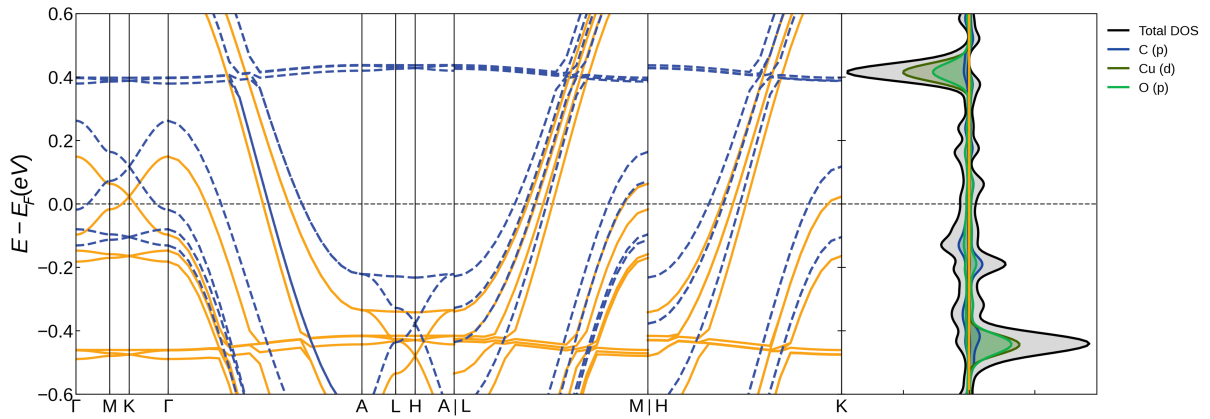


**Figure 5** – Absorption spectra for three SBUs connected to the linker. The structures are in monolayer, parallel, and sliding orientations.

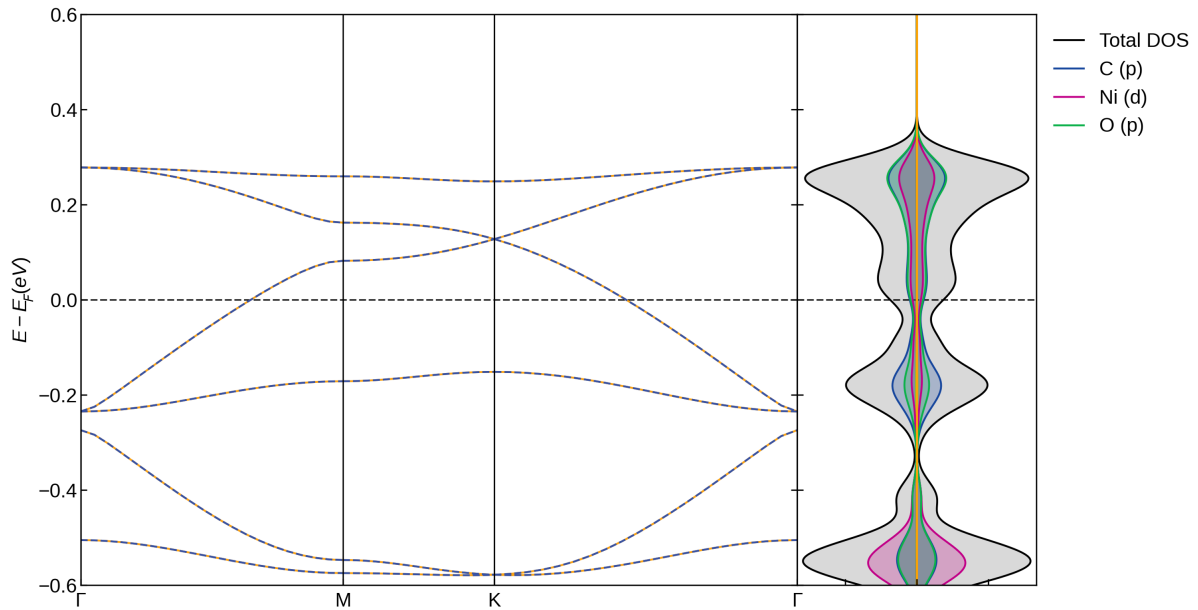
# Band Structure Calculations



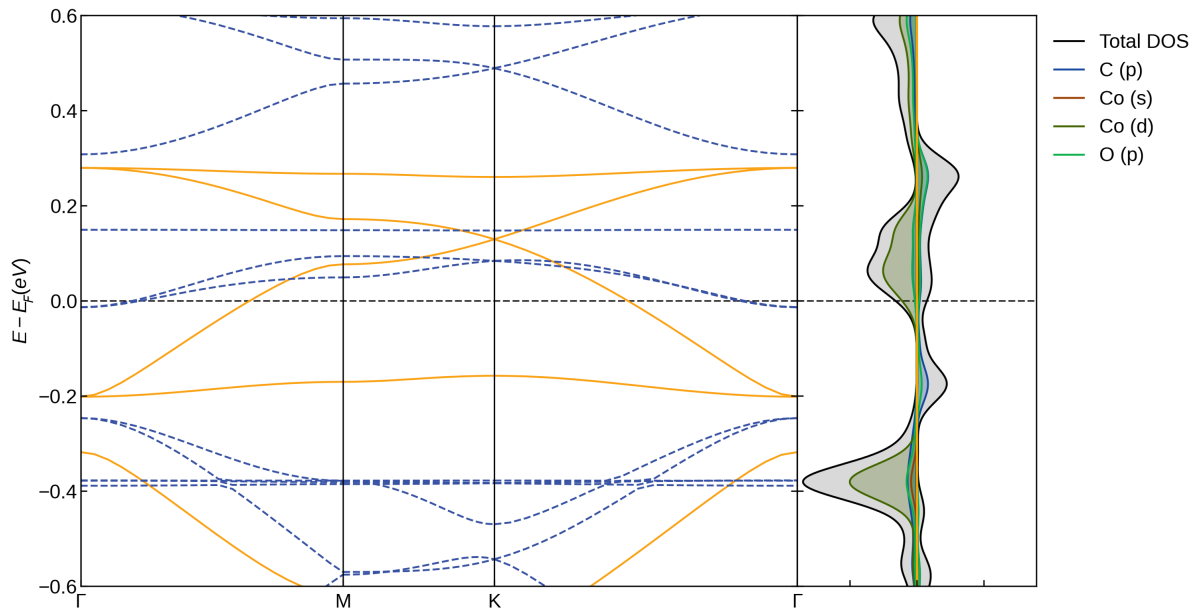
**Figure 6** – The band structure of a fully relaxed 3D model of  $Cu_3(HHTP)_2$  (optimization of unit cell parameters and atomic positions) in a high-spin state. Solid lines are spin up and dashed lines are spin down. The Fermi energy is set to zero.



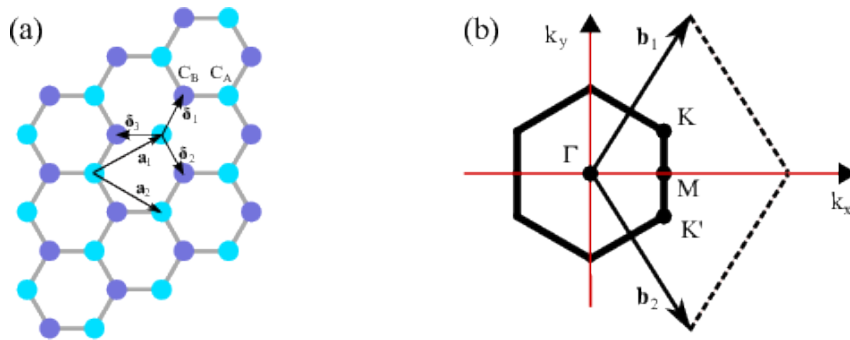
**Figure 7** – The band structure of a 3D model of  $Cu_3(HHTP)_2$  where the planes were confined to remain in hexagonal symmetry while unit cell parameters and atomic positions were optimized in a high-spin state. Solid lines are spin up, and dashed lines are spin down. The Fermi energy is set to zero.



**Figure 8** – The band structure of a fully relaxed 2D model of  $Ni_3(HHTP)_2$  (optimization of unit cell parameters and atomic positions) in a high-spin state. Solid lines are spin up and dashed lines are spin down. The Fermi energy is set to zero.

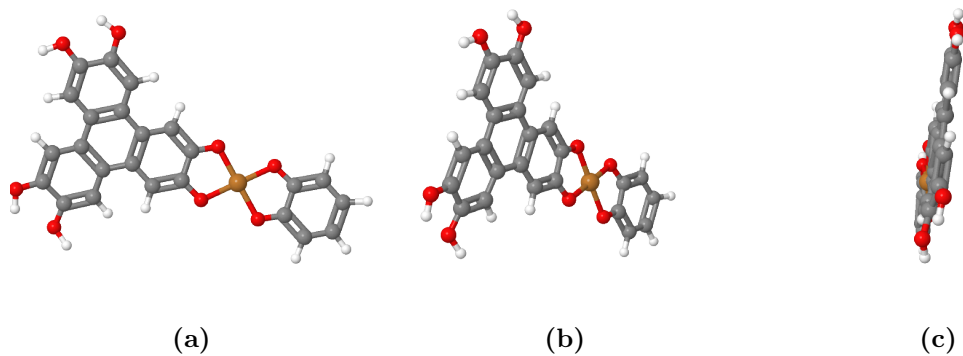


**Figure 9** – The band structure of a fully relaxed 2D model of  $Co_3(HHTP)_2$  (optimization of unit cell parameters and atomic positions) in a high-spin state. Solid lines are spin up and dashed lines are spin down. The Fermi energy is set to zero.

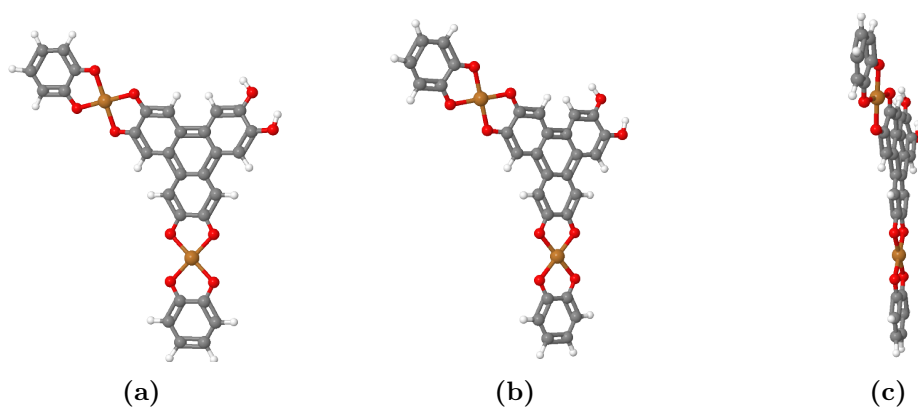


**Figure 10** – Honeycomb lattice and its Brillouin zone. (a) Lattice structure of graphene, composed of two interpenetrating triangular lattices ( $a_1$  and  $a_2$  are the lattice unit vectors, and  $\delta_i$ ,  $i = 1, 2, 3$  are the nearest-neighbor vectors). (b) Corresponding Brillouin zone. The Dirac cones are located at the  $K$  and  $K'$  points. The sketch figure is taken from Ref.[15]

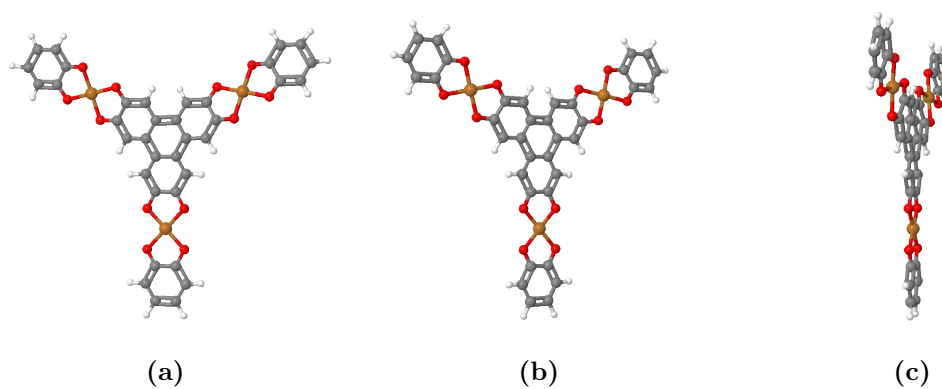
## Extracted fragments of $Cu_3(HHTP)_2$ used for UV-vis spectra calculation



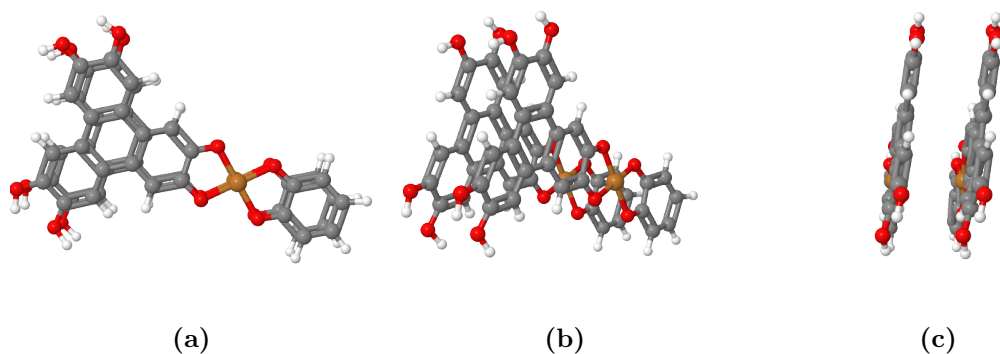
**Figure 11** – The monolayer considering one SBU at a) top, b) 45° rotation and c) side view.



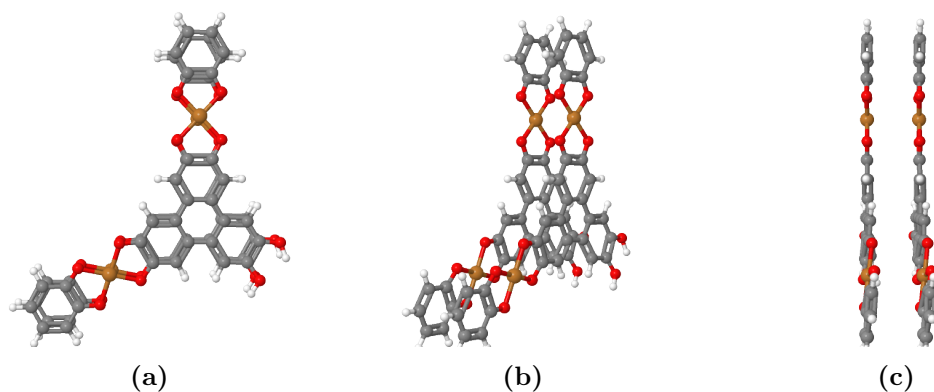
**Figure 12** – The monolayer considering two SBUs at a) top, b) 45° rotation and c) side view.



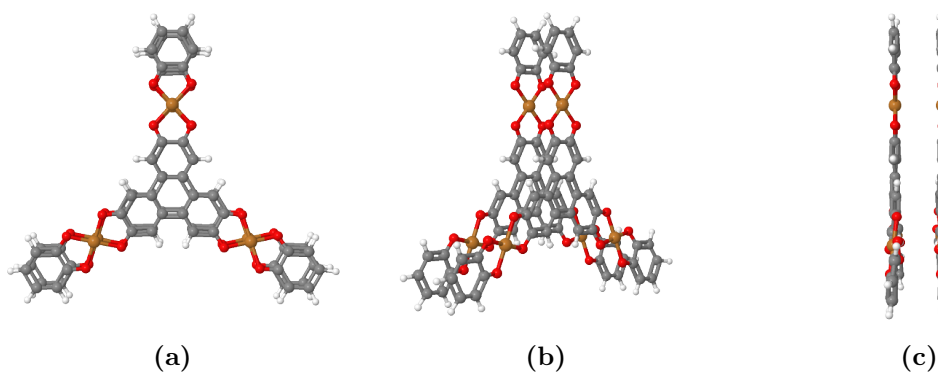
**Figure 13** – The monolayer considering three SBUs at a) top, b) 45° rotation and c) side view.



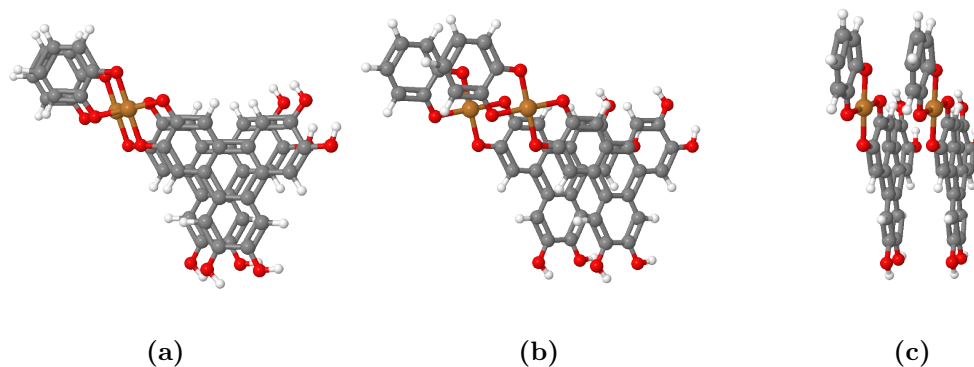
**Figure 14** – The double-layer model with parallel orientation of the layers considering one SBU at a) top, b) 45° rotation and c) side view. The fragments were extracted from the periodically optimized  $Cu_3(HHTP)_2$ .



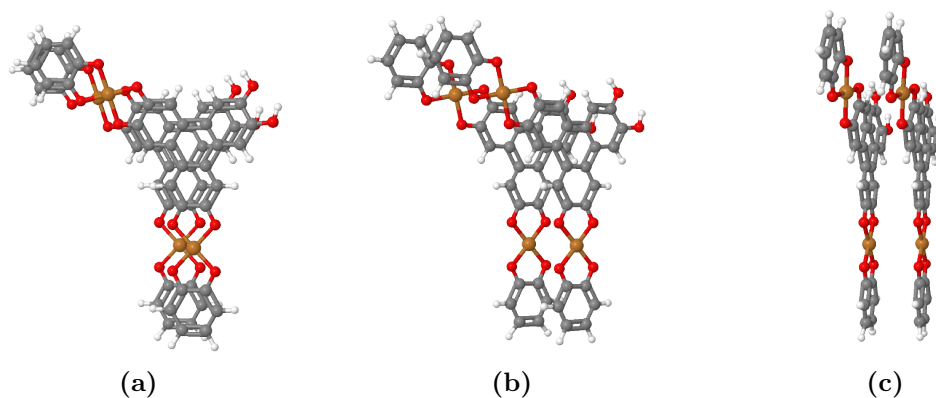
**Figure 15** – The double-layer model with parallel orientation of the layers considering two SBUs at a) top, b) 45° rotation and c) side view. The fragments were extracted from the periodically optimized  $Cu_3(HHTP)_2$ .



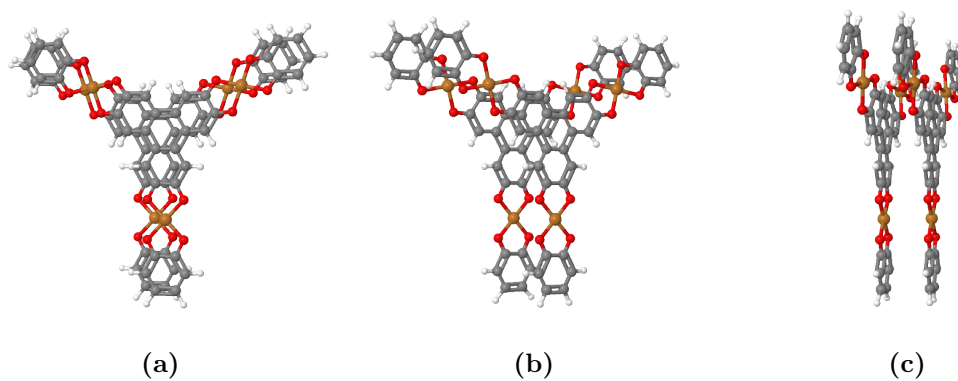
**Figure 16** – The double-layer model with parallel orientation of the layers considering three SBUs at a) top, b) 45° rotation and c) side view. The fragments were extracted from the periodically optimized  $Cu_3(HHTP)_2$ .



**Figure 17** – The double-layer model with sliding orientation of the layers considering one SBU at a) top, b) 45°rotation and c) side view. The fragments were extracted from the periodically optimized  $Cu_3(HHTP)_2$ .



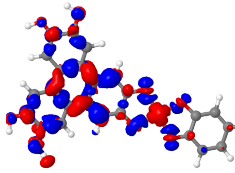
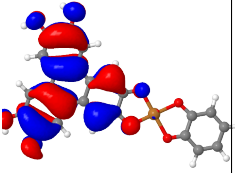
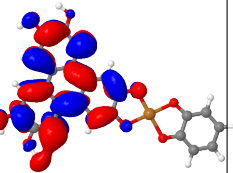
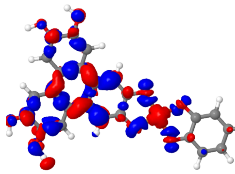
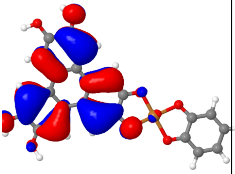
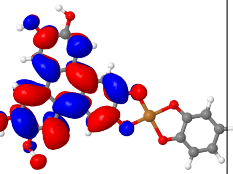
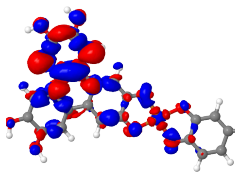
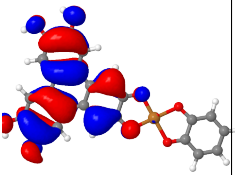
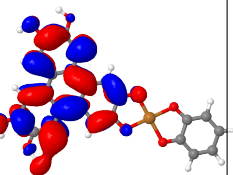
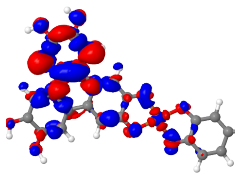
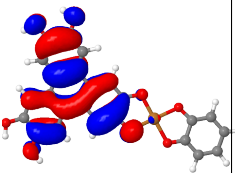
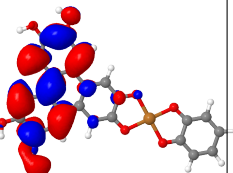
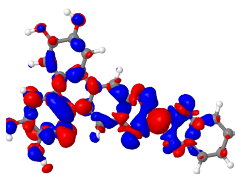
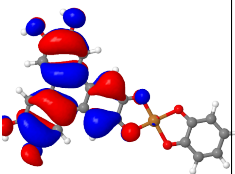
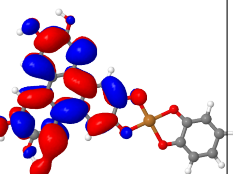
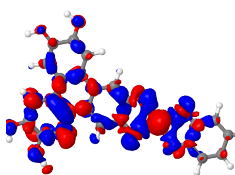
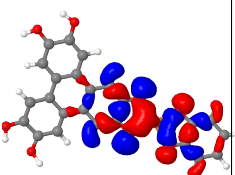
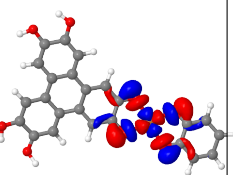
**Figure 18** – The double-layer model with sliding orientation of the layers considering two SBUs at a) top, b) 45°rotation and c) side view. The fragments were extracted from the periodically optimized  $Cu_3(HHTP)_2$ .



**Figure 19** – The double-layer model with sliding orientation of the layers considering three SBUs at a) top, b) 45°rotation and c) side view. The fragments were extracted from the periodically optimized  $Cu_3(HHTP)_2$ .

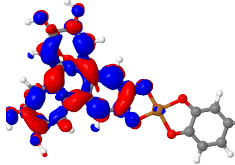
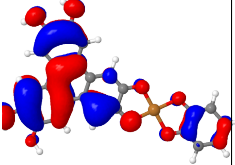
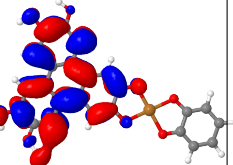
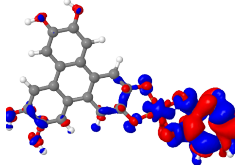
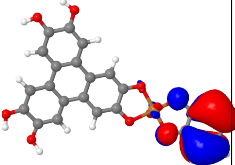
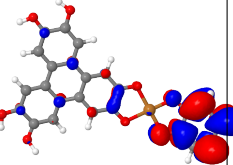
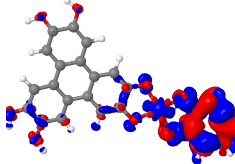
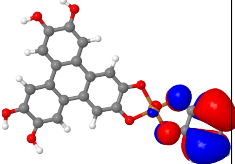
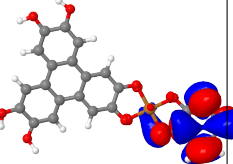
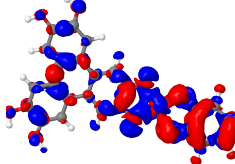
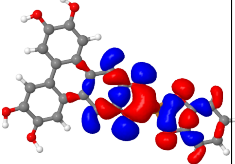
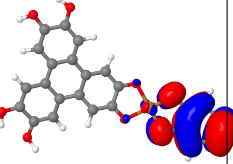
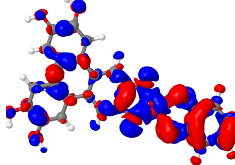
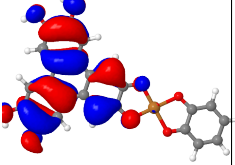
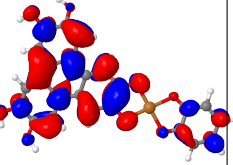
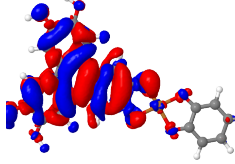
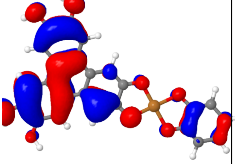
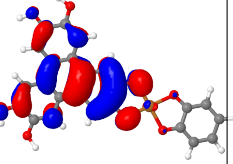
## Analysis of transition orbitals

**Table 1** – Molecular orbitals and electron density differences for excitations of a monolayer with one SBU.

	Ex. No.	Wave-length (nm)	occ. orbital	virt. orbital	Cont (%)	EDD	OCC	VIRT
0	43	265.2	126	129	12.8			
1	43	265.2	123	128	18.0			
2	33	296.4	126	129	11.7			
3	33	296.4	124	129	20.4			
4	32	299.9	126	129	11.3			
5	32	299.9	118	127	21.9			

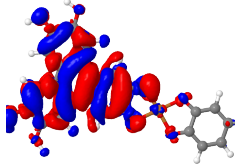
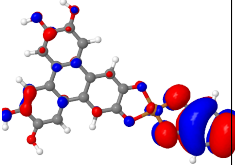
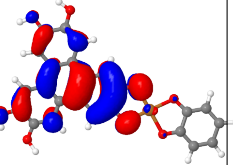
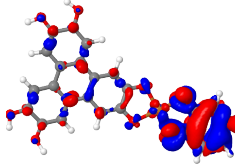
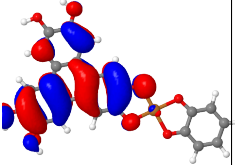
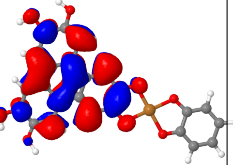
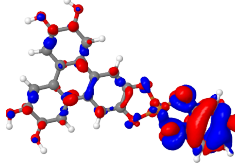
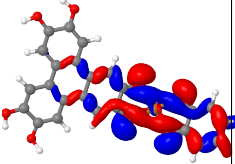
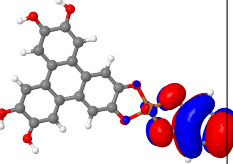
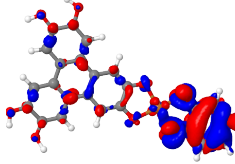
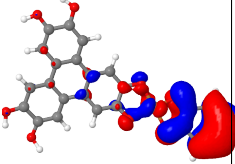
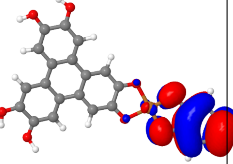
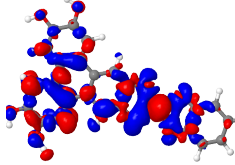
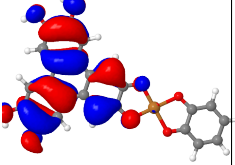
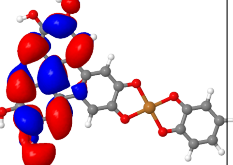
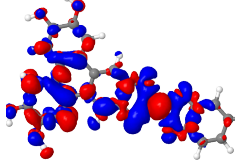
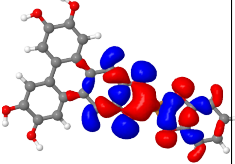
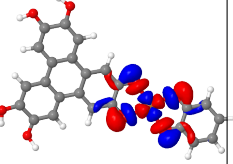
Continued on next page

**Table 1** – Molecular orbitals and electron density differences for excitations of a monolayer with one SBU.

	Ex. No.	Wave-length (nm)	occ. orbital	virt. orbital	Cont (%)	EDD	OCC	VIRT
6	73	219.6	124	129	13.7			
7	114	192.6	122	130	18.2			
8	114	192.6	122	134	25.9			
9	42	267.3	118	126	12.7			
10	42	267.3	126	131	16.2			
11	7	554.9	124	127	57.5			

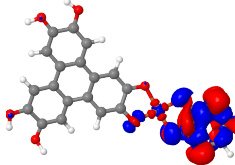
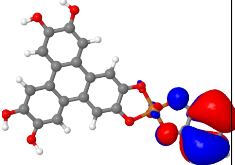
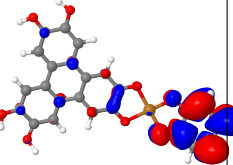
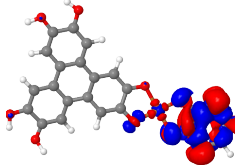
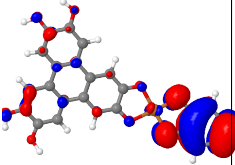
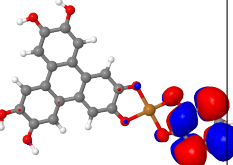
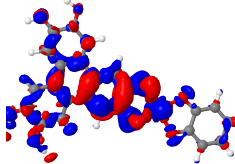
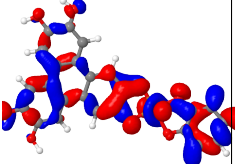
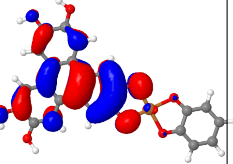
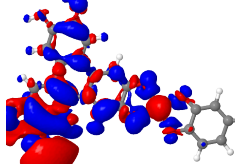
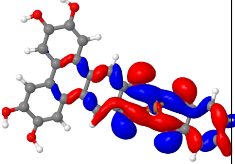
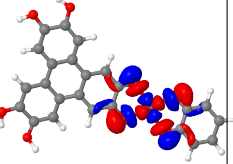
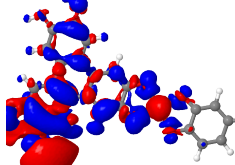
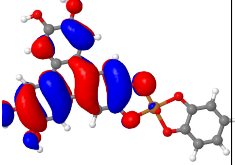
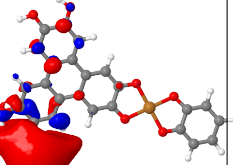
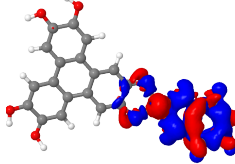
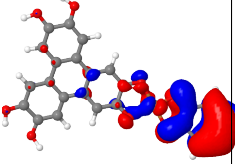
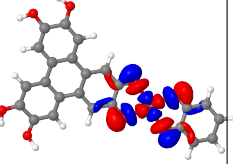
Continued on next page

**Table 1** – Molecular orbitals and electron density differences for excitations of a monolayer with one SBU.

	Ex. No.	Wave-length (nm)	occ. orbital	virt. orbital	Cont (%)	EDD	OCC	VIRT
12	7	554.9	125	127	12.7			
13	22	340.1	125	130	11.5			
14	22	340.1	116	126	16.7			
15	22	340.1	115	126	20.6			
16	31	302.5	126	128	20.6			
17	31	302.5	118	127	30.9			

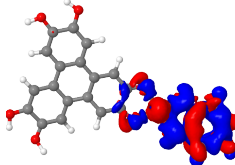
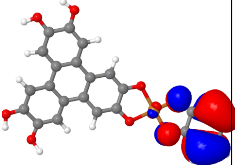
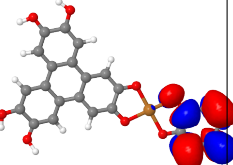
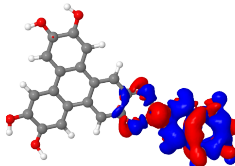
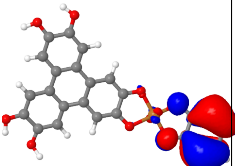
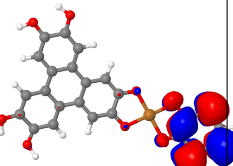
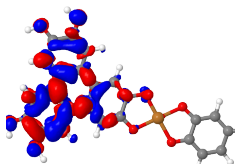
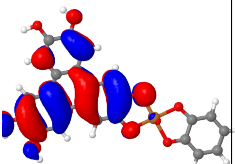
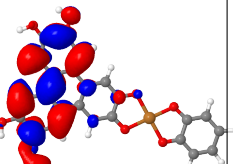
Continued on next page

**Table 1** – Molecular orbitals and electron density differences for excitations of a monolayer with one SBU.

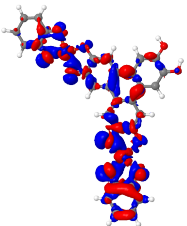
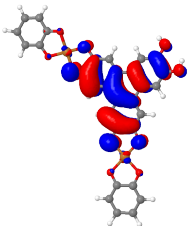
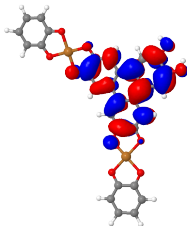
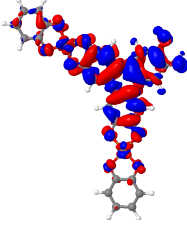
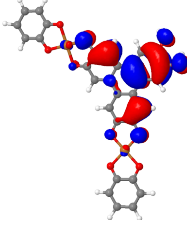
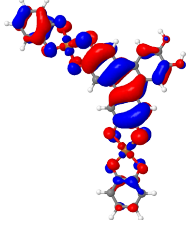
	Ex. No.	Wave-length (nm)	occ. orbital	virt. orbital	Cont (%)	EDD	OCC	VIRT
18	39	278.1	122	130	17.0			
19	39	278.1	125	133	48.0			
20	105	195.7	106	127	15.3			
21	46	252.7	116	127	15.8			
22	46	252.7	125	131	23.5			
23	119	190.0	115	127	16.7			

Continued on next page

**Table 1** – Molecular orbitals and electron density differences for excitations of a monolayer with one SBU.

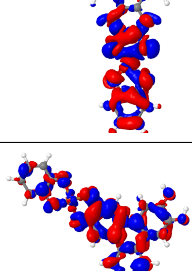
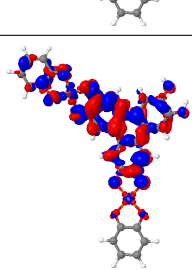
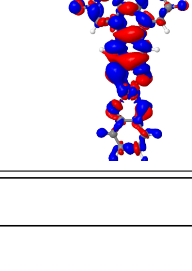
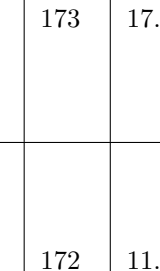
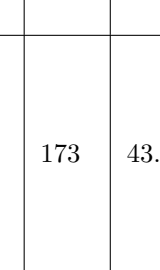
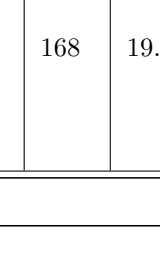
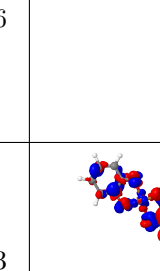
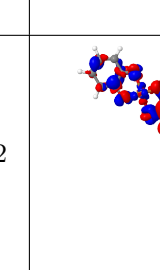
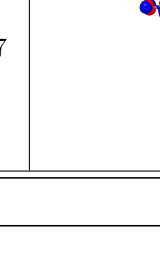
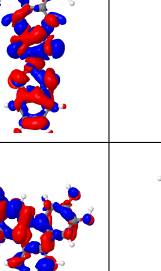
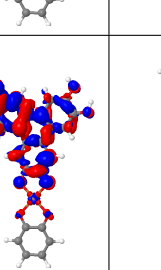
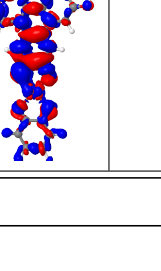
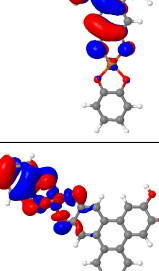
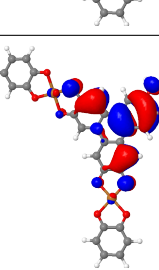
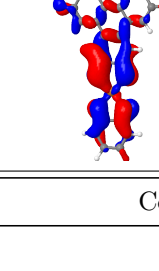
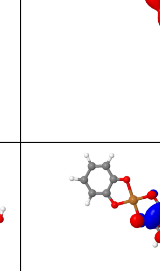
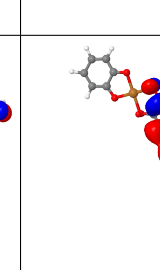
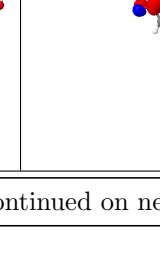
	Ex. No.	Wave-length (nm)	occ. orbital	virt. orbital	Cont (%)	EDD	OCC	VIRT
24	119	190.0	122	135	13.5			
25	119	190.0	122	133	14.0			
26	28	315.2	125	129	22.7			

**Table 2** – Molecular orbitals and electron density differences for excitations of a monolayer with two SBUs.

	Ex. No.	Wave-length (nm)	occ. orbital	virt. orbital	Cont (%)	EDD	OCC	VIRT
0	32	338.1	167	172	20.3			
1	11	582.3	164	168	74.7			

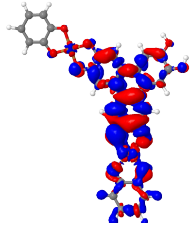
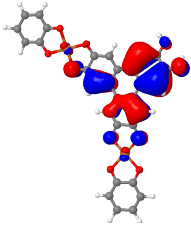
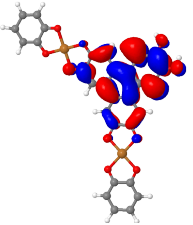
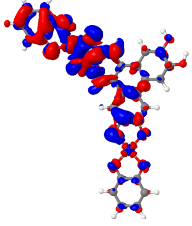
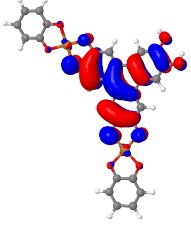
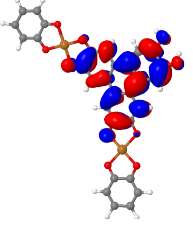
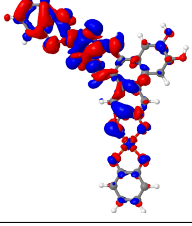
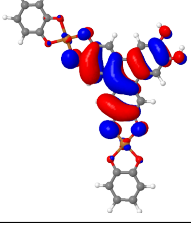
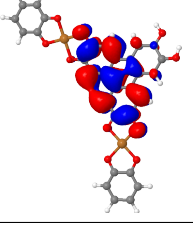
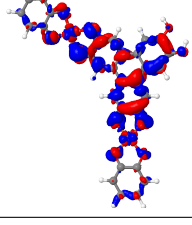
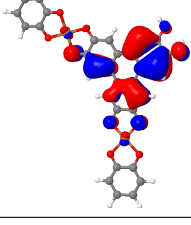
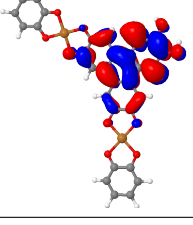
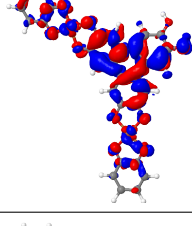
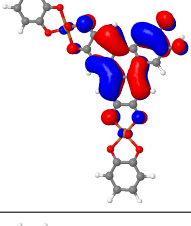
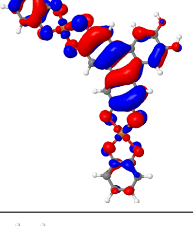
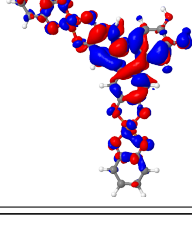
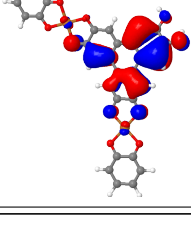
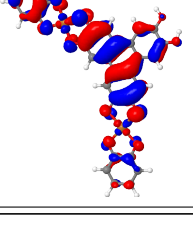
Continued on next page

**Table 2** – Molecular orbitals and electron density differences for excitations of a monolayer with two SBUs.

	Ex. No.	Wave-length (nm)	occ. orbital	virt. orbital	Cont (%)	EDD	OCC	VIRT
2	33	335.9	167	171	44.1			
3	35	309.8	167	172	12.4			
4	35	309.8	167	173	17.6			
5	94	215.9	165	172	11.3			
6	94	215.9	164	173	43.2			
7	104	205.8	139	168	19.7			

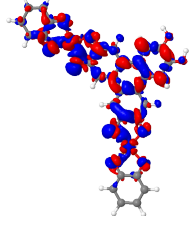
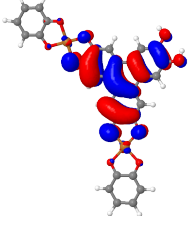
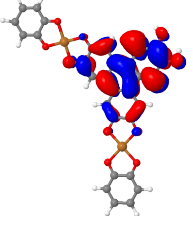
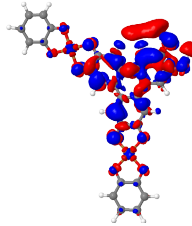
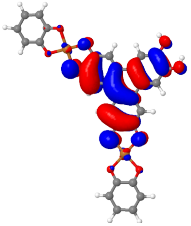
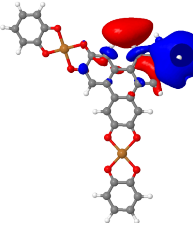
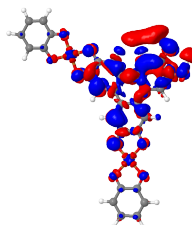
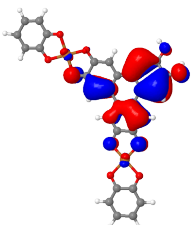
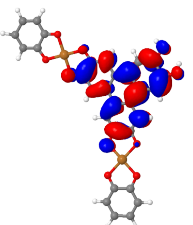
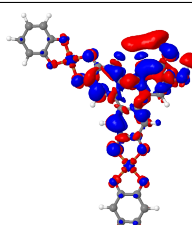
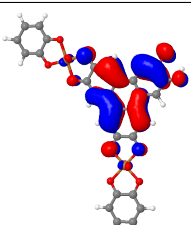
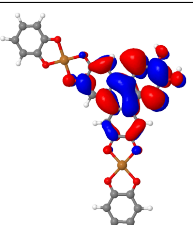
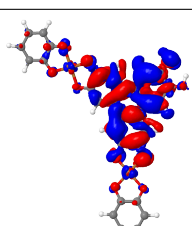
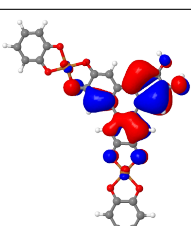
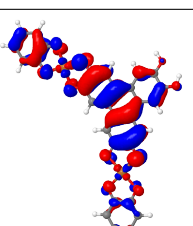
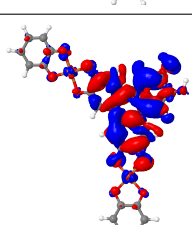
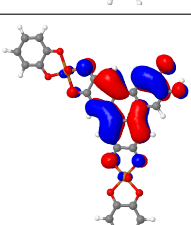
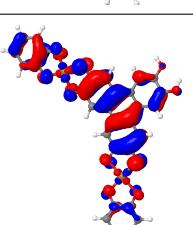
Continued on next page

**Table 2** – Molecular orbitals and electron density differences for excitations of a monolayer with two SBUs.

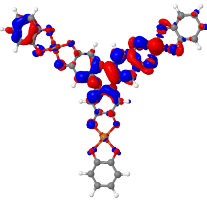
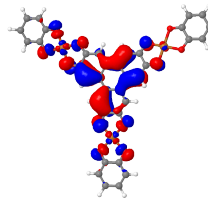
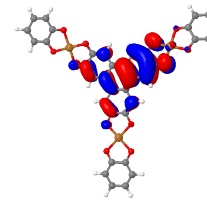
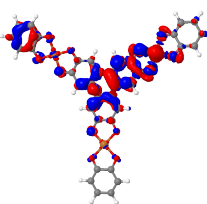
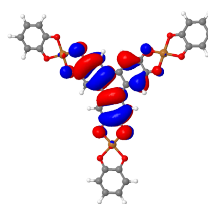
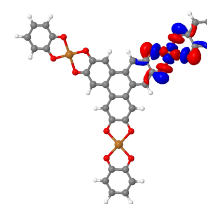
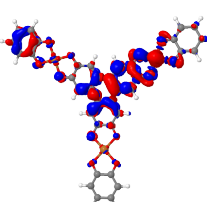
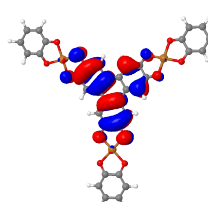
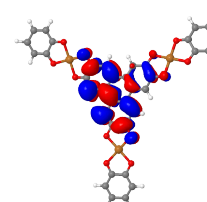
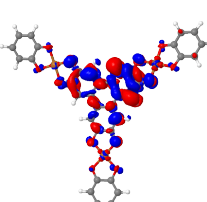
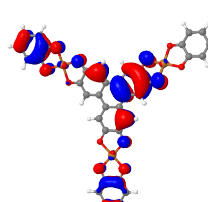
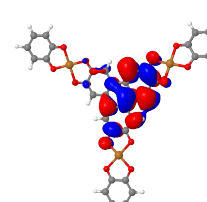
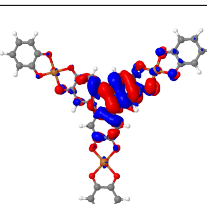
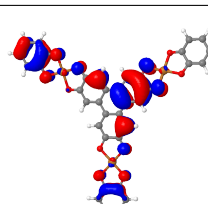
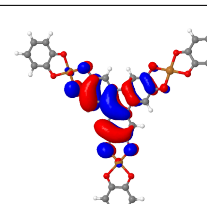
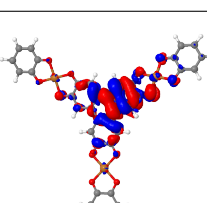
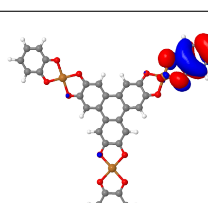
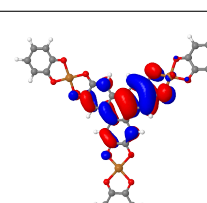
	Ex. No.	Wave-length (nm)	occ. orbital	virt. orbital	Cont (%)	EDD	OCC	VIRT
8	104	205.8	160	171	11.9			
9	36	308.0	167	172	13.9			
10	36	308.0	167	173	27.6			
11	107	204.3	160	171	20.5			
12	22	425.1	159	168	11.9			
13	22	425.1	160	168	34.6			

Continued on next page

**Table 2** – Molecular orbitals and electron density differences for excitations of a monolayer with two SBUs.

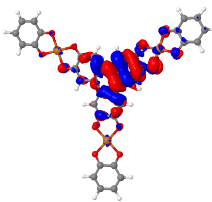
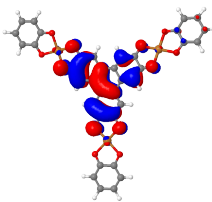
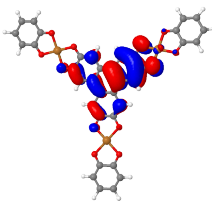
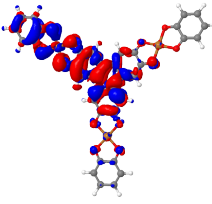
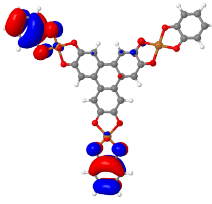
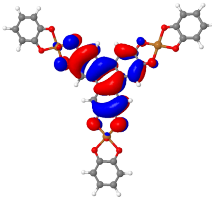
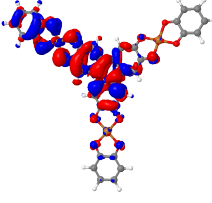
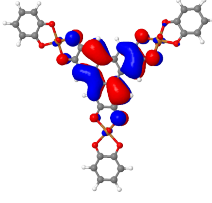
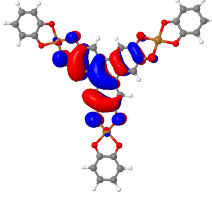
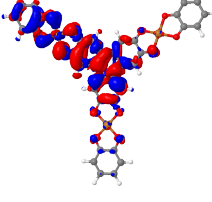
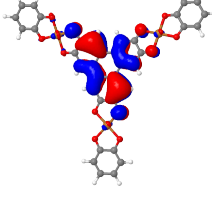
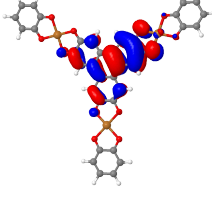
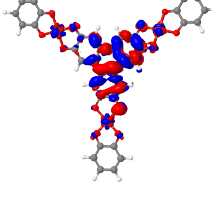
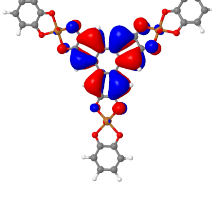
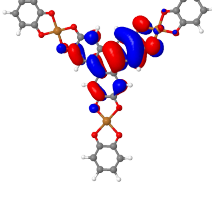
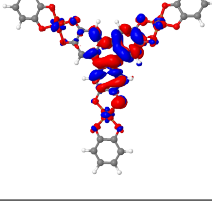
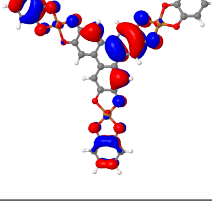
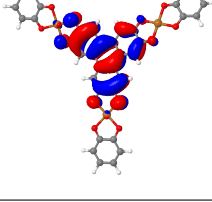
	Ex. No.	Wave-length (nm)	occ. orbital	virt. orbital	Cont (%)	EDD	OCC	VIRT
14	34	316.2	167	171	33.8			
15	112	201.2	167	183	10.4			
16	112	201.2	160	172	22.6			
17	112	201.2	159	171	25.4			
18	25	414.0	160	168	22.8			
19	25	414.0	159	168	41.2			

**Table 3** – Molecular orbitals and electron density differences for excitations of a monolayer with three SBU.

	Ex. No.	Wave-length (nm)	occ. orbital	virt. orbital	Cont (%)	EDD	OCC	VIRT
0	49	343.1	201	210	11.6			
1	49	343.1	209	213	11.7			
2	49	343.1	209	214	12.7			
3	86	289.3	208	215	32.7			
4	19	558.5	208	209	12.3			
5	19	558.5	208	210	13.2			

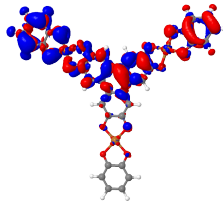
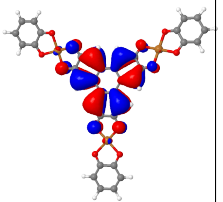
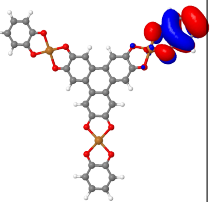
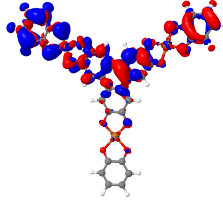
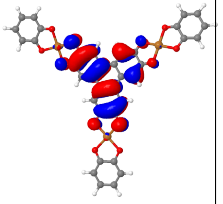
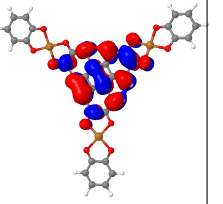
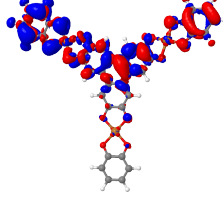
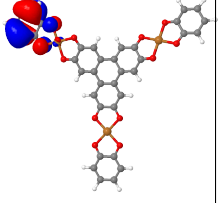
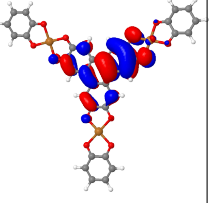
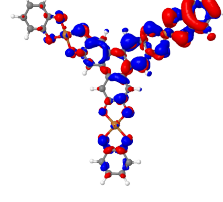
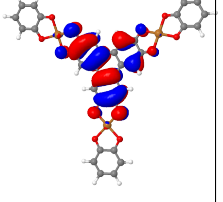
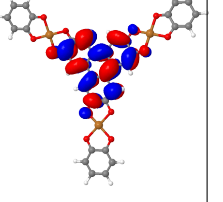
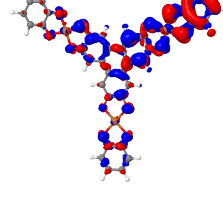
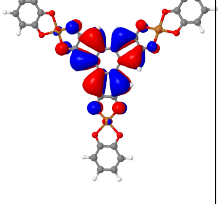
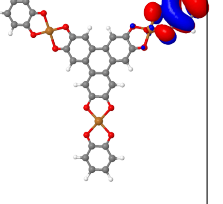
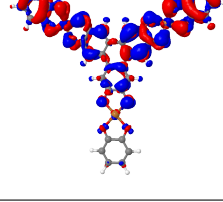
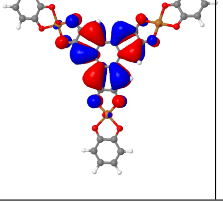
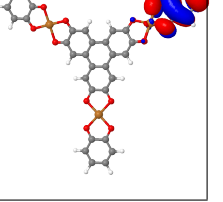
Continued on next page

**Table 3** – Molecular orbitals and electron density differences for excitations of a monolayer with three SBU.

	Ex. No.	Wave-length (nm)	occ. orbital	virt. orbital	Cont (%)	EDD	OCC	VIRT
6	19	558.5	207	210	35.4			
7	46	375.7	207	210	16.6			
8	46	375.7	200	209	18.5			
9	46	375.7	202	210	19.2			
10	14	591.8	206	210	15.3			
11	14	591.8	208	210	30.8			

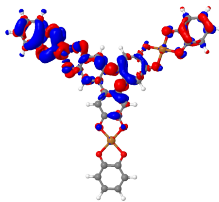
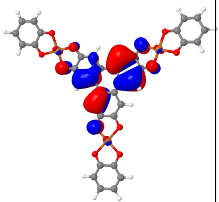
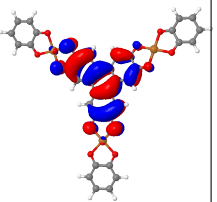
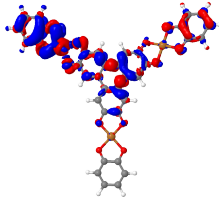
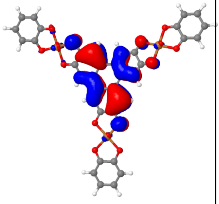
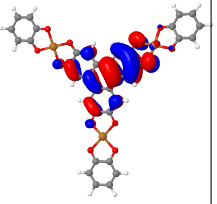
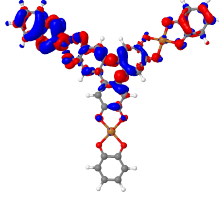
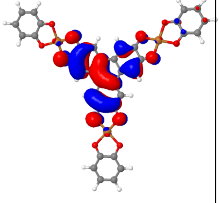
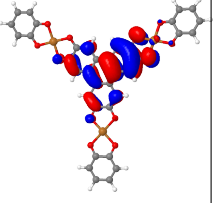
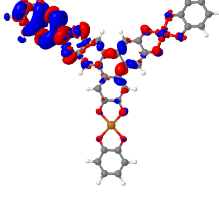
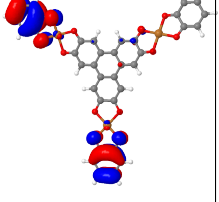
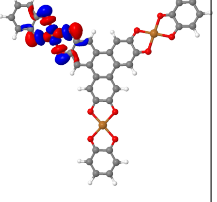
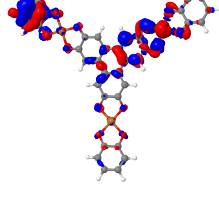
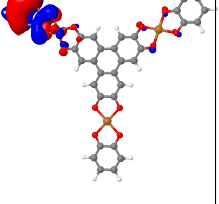
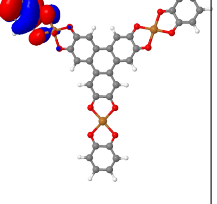
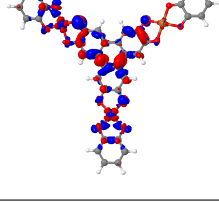
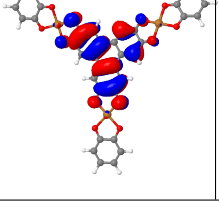
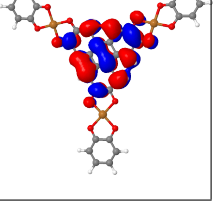
Continued on next page

**Table 3** – Molecular orbitals and electron density differences for excitations of a monolayer with three SBU.

	Ex. No.	Wave-length (nm)	occ. orbital	virt. orbital	Cont (%)	EDD	OCC	VIRT
12	69	310.4	205	211	13.4			
13	69	310.4	209	216	12.5			
14	69	310.4	205	210	27.3			
15	68	312.5	209	215	20.8			
16	68	312.5	205	211	22.6			
17	66	313.6	205	211	24.9			

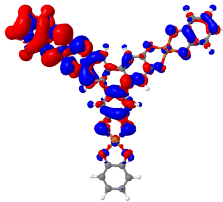
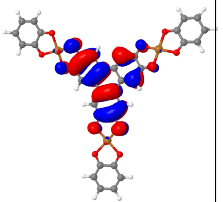
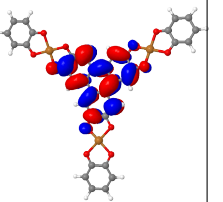
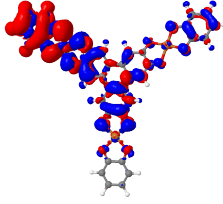
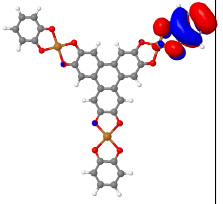
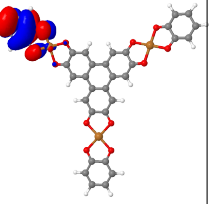
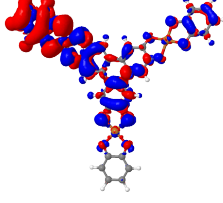
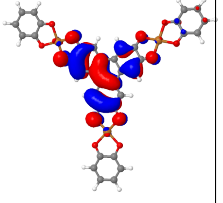
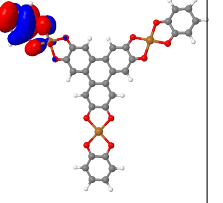
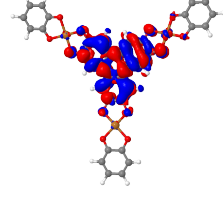
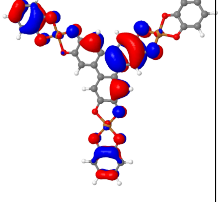
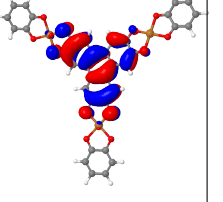
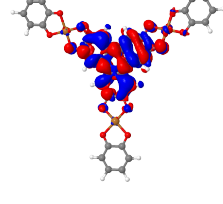
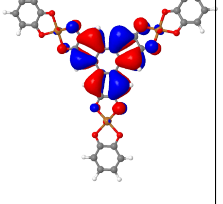
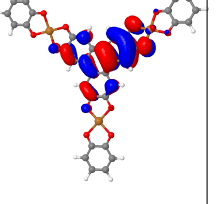
Continued on next page

**Table 3** – Molecular orbitals and electron density differences for excitations of a monolayer with three SBU.

	Ex. No.	Wave-length (nm)	occ. orbital	virt. orbital	Cont (%)	EDD	OCC	VIRT
18	40	411.5	201	210	14.5			
19	40	411.5	202	210	14.8			
20	40	411.5	207	210	15.3			
21	38	413.6	207	212	22.3			
22	52	337.3	192	212	24.1			
23	87	287.3	209	216	14.7			

Continued on next page

**Table 3** – Molecular orbitals and electron density differences for excitations of a monolayer with three SBU.

	Ex. No.	Wave-length (nm)	occ. orbital	virt. orbital	Cont (%)	EDD	OCC	VIRT
24	65	314.3	209	215	15.7			
25	65	314.3	208	212	20.8			
26	65	314.3	207	212	27.4			
27	7	680.1	208	210	18.9			
28	7	680.1	206	210	49.3			

## Periodically optimized structure of $Cu_3(HHTP)_2$

C	Cu	H	O
1.000000000000000			
21.0950327475553365	-0.0401271721131145		4.9353538830025370
-10.5129869811262520	18.9346090134835805		-2.4933420680299774
0.7489014317924431	-0.0078902131700095		3.4816115023252268
C	Cu	H	O
36	3	12	12
Direct			
0.5993321438093584	0.4640001942355294	0.0370611694610398	
0.8609313014485890	0.3975782308350186	0.0273524040763195	
0.1347236747647887	0.5359707166956628	0.0474596551515373	
0.1995117458104362	0.5375594667375462	0.0544704493981046	
0.2670696454498386	0.6012318378091921	0.0099161431405395	
0.7950801094391357	0.3335825306449500	0.0402652439615025	
0.7322277478155770	0.3319595310722565	0.0098996905380928	
0.6658962466981673	0.2655235045036803	0.0054650104322982	
0.6658908301833713	0.2011550035246364	0.9968608383447146	
0.6013208891228863	0.1363756162517861	0.0060795272607915	
0.5333159598656737	0.1364518187368738	0.0135275826462082	
0.5342107452092379	0.2013819740294215	0.0161371612486649	
0.5991123825782039	0.2655975064900002	0.0015055992098163	
0.6620839646371963	0.4624166009355247	0.0499143974444415	
0.6658220853269377	0.3987106306458692	0.0081980996392598	
0.5998820903280878	0.3321229989557820	0.9911026476061952	
0.8653057858524522	0.4636355036092916	0.9573976355069647	
0.5390213098048451	0.3338254229915388	0.9570880691397979	
0.1388415148789295	0.6020111142166537	0.9790245041237378	
0.2674872798853379	0.6678358134716812	0.9962787632406608	
0.4027193916770633	0.5364076307196703	0.9424495427832822	
0.3395197530408226	0.5378981422098413	0.9349441923711215	
0.3349683340577136	0.6013835022387538	0.9861809152994642	
0.4006052645414037	0.6680567856728894	0.0063816977369232	
0.4620517458821002	0.6664498123630872	0.0337199419803656	
0.4642555813864447	0.6024435314073014	0.0152446306967240	
0.2045419205855638	0.6661031972263217	0.9669266723361450	
0.4004354261714554	0.7344910831703163	0.0059943208537755	
0.4648772173641508	0.8636520909215695	0.0079859991643020	
0.7331712092354128	0.3986158030390817	0.9913829070587548	
0.8008268284321280	0.4621715836210099	0.9471821712503937	
0.3966915207119801	0.8635244044524711	0.0167778981627993	
0.3325990040686026	0.7985824199771231	0.0207953951344953	
0.3333809315089698	0.7343690142550983	0.0048576921883811	
0.4647683175086558	0.7988678629045906	0.9978221342920641	
0.5375615552370858	0.3979203256375853	0.9669629702387034	
0.5013074280607789	0.5002456434368243	0.9868572333845808	
0.9998993593938670	0.4997075153078628	0.0030870931987276	
0.4986663287031143	0.0000017418183347	0.0146063413897108	
0.1952970247300986	0.4875362941975128	0.0982981272639671	
0.8054180875595943	0.5122274371948232	0.9006913046088720	
0.7957305059618259	0.2855655820558274	0.0751104971694799	
0.2036712541865084	0.7140830435662489	0.9335960728314113	
0.2827002409742629	0.8007783332760174	0.0327431627034102	
0.5169576123698917	0.8013375199032129	0.9864907254872661	
0.5105929986445485	0.7144456263362980	0.0709259577584970	
0.2941318743440454	0.4878980912835909	0.8861255399507172	
0.7155209655823173	0.1987407117096551	0.9872385315464847	

0.4822312089291884	0.1991621777596472	0.0260181145284103
0.4903285119876983	0.2857872133704236	0.9218088279604580
0.7076586920782866	0.5125131833154595	0.0961083599564284
0.5182352567369898	0.5980254330390212	0.0568972343414617
0.5221927681290007	0.9247368517078769	0.0109639245003172
0.9305228514619317	0.5201733520756505	0.9030742815098941
0.0805646975500347	0.5974669209928190	0.9353017258069581
0.4839751597883344	0.4023763135921570	0.9208271793380297
0.9191836043978021	0.4020284511285575	0.0712491088572275
0.0695411907284201	0.4794134936863035	0.1022548116370792
0.5974655041098361	0.0752899447195580	0.0100233738735209
0.4756045303163388	0.0754412314903805	0.0150008268532434
0.5909899495196032	0.5207191010425115	0.0888589730665351
0.3999374313371011	0.9245213546078962	0.0186591728231198
0.4116335063789225	0.4799142310998674	0.8844169473929793

# Bibliography

- [1] G. Kresse and J. Furthmüller. “Efficiency of Ab-Initio Total Energy Calculations for Metals and Semiconductors Using a Plane-Wave Basis Set”. In: *Computational Materials Science* 6.1 (July 1, 1996), pp. 15–50. ISSN: 0927-0256. DOI: [https://doi.org/10.1016/0927-0256\(96\)00008-0](https://doi.org/10.1016/0927-0256(96)00008-0). URL: <https://www.sciencedirect.com/science/article/pii/0927025696000080> (visited on 02/16/2022).
- [2] John P. Perdew, Kieron Burke, and Matthias Ernzerhof. “Generalized Gradient Approximation Made Simple”. In: *Physical Review Letters* 77.18 (10), pp. 3865–3868. DOI: [10.1103/PhysRevLett.77.3865](https://doi.org/10.1103/PhysRevLett.77.3865).
- [3] T. Gould and T. Bucko. “C6 Coefficients and Dipole Polarizabilities for All Atoms and Many Ions in Rows 1–6 of the Periodic Table”. In: *Journal of Chemical Theory and Computation* 12 (June 2016), pp. 3603–3613. DOI: [10.1021/acs.jctc.6b00361](https://doi.org/10.1021/acs.jctc.6b00361). URL: <https://pubs.acs.org/doi/10.1021/acs.jctc.6b00361> (visited on 02/13/2025).
- [4] T. Gould et al. “A Fractionally Ionic Approach to Polarizability and van der Waals Many-Body Dispersion Calculations”. In: *Journal of Chemical Theory and Computation* 12 (Nov. 2016), pp. 5920–5930. DOI: [10.1021/acs.jctc.6b00925](https://doi.org/10.1021/acs.jctc.6b00925). URL: <https://pubs.acs.org/doi/10.1021/acs.jctc.6b00925> (visited on 02/13/2025).
- [5] Sree Ganesh Balasubramani et al. “TURBOMOLE: Modular program suite for ab initio quantum-chemical and condensed-matter simulations”. In: *The Journal of Chemical Physics* 152.18 (May 2020), p. 184107. ISSN: 0021-9606. DOI: [10.1063/5.0004635](https://doi.org/10.1063/5.0004635). eprint: [https://pubs.aip.org/aip/jcp/article-pdf/doi/10.1063/5.0004635/16685296/184107\\_1\\_online.pdf](https://pubs.aip.org/aip/jcp/article-pdf/doi/10.1063/5.0004635/16685296/184107_1_online.pdf). URL: <https://doi.org/10.1063/5.0004635>.
- [6] Filipp Furche and Dmitrij Rappoport. “III - Density Functional Methods for Excited States: Equilibrium Structure and Electronic Spectra”. In: *Theoretical and Computational Chemistry*. Ed. by M. Olivucci. Vol. 16. Computational Photochemistry. Elsevier, Jan. 2005, pp. 93–128. DOI: [10.1016/S1380-7323\(05\)80020-2](https://doi.org/10.1016/S1380-7323(05)80020-2). (Visited on 03/08/2024).
- [7] E. J. Baerends, D. E. Ellis, and P. Ros. “Self-consistent molecular Hartree-Fock-Slater calculations I. The computational procedure”. In: *Chemical Physics* 2.1 (Sept. 1973), pp. 41–51. ISSN: 0301-0104. DOI: [10.1016/0301-0104\(73\)80059-X](https://doi.org/10.1016/0301-0104(73)80059-X). URL: <https://www.sciencedirect.com/science/article/pii/030101047380059X> (visited on 03/08/2024).

- [8] B. I. Dunlap, J. W. D. Connolly, and J. R. Sabin. “On some approximations in applications of  $X\alpha$  theory”. In: *The Journal of Chemical Physics* 71.8 (Oct. 1979), pp. 3396–3402. ISSN: 0021-9606. DOI: [10.1063/1.438728](https://doi.org/10.1063/1.438728). URL: <https://doi.org/10.1063/1.438728> (visited on 03/08/2024).
- [9] Karin Eichkorn et al. “Auxiliary basis sets for main row atoms and transition metals and their use to approximate Coulomb potentials”. en. In: *Theoretical Chemistry Accounts* 97.1 (Oct. 1997), pp. 119–124. ISSN: 1432-2234. DOI: [10.1007/s002140050244](https://doi.org/10.1007/s002140050244). URL: <https://doi.org/10.1007/s002140050244> (visited on 03/08/2024).
- [10] Michael Kühn and Florian Weigend. “Implementation of Two-Component Time-Dependent Density Functional Theory in TURBOMOLE”. In: *Journal of Chemical Theory and Computation* 9.12 (Dec. 2013), pp. 5341–5348. ISSN: 1549-9618. DOI: [10.1021/ct400743r](https://doi.org/10.1021/ct400743r). (Visited on 03/08/2024).
- [11] Christof Hättig and Florian Weigend. “CC2 excitation energy calculations on large molecules using the resolution of the identity approximation”. In: *The Journal of Chemical Physics* 113.13 (Oct. 2000), pp. 5154–5161. ISSN: 0021-9606. DOI: [10.1063/1.1290013](https://doi.org/10.1063/1.1290013). URL: <https://doi.org/10.1063/1.1290013> (visited on 03/08/2024).
- [12] Florian Weigend and Reinhart Ahlrichs. “Balanced Basis Sets of Split Valence, Triple Zeta Valence and Quadruple Zeta Valence Quality for H to Rn: Design and Assessment of Accuracy”. In: *Physical Chemistry Chemical Physics* 7.18 (2005), pp. 3297–3305. ISSN: 1463-9076. DOI: [10.1039/B508541A](https://doi.org/10.1039/B508541A).
- [13] Mark E. Casida. “Time-Dependent Density Functional Response Theory for Molecules”. In: *Recent Advances in Computational Chemistry*. Vol. 1. WORLD SCIENTIFIC, Nov. 1995, pp. 155–192. ISBN: 978-981-02-2442-4 978-981-283-058-6. DOI: [10.1142/9789812830586\\_0005](https://doi.org/10.1142/9789812830586_0005). (Visited on 05/03/2020).
- [14] Michael Kühn and Florian Weigend. “Phosphorescence lifetimes of organic light-emitting diodes from two-component time-dependent density functional theory”. In: *The Journal of Chemical Physics* 141.22 (Dec. 2014), p. 224302. ISSN: 0021-9606. DOI: [10.1063/1.4902013](https://doi.org/10.1063/1.4902013). URL: <https://doi.org/10.1063/1.4902013> (visited on 04/11/2024).
- [15] Mahdi Moradinasab. “Optical Properties of Semiconductor Nanostructures”. PhD thesis. Leomathausergasse 69/2 1230 Wien, Österreich: Technischen Universität Wien, Mar. 2015.